Proc. Natl. Acad. Sci. USA
Vol. 95, pp. 7103–7108, June 1998
Neurobiology

Disease sequence from mutant *rhodopsin* allele to rod and cone photoreceptor degeneration in man

ARTUR V. CIDECIYAN*†, DONALD C. HOOD‡, YIJUN HUANG*, EYAL BANIN*, ZONG-YI LI§, EDWIN M. STONE¶, ANN H. MILAM§, AND SAMUEL G. JACOBSON*

*Scheie Eye Institute, Department of Ophthalmology, University of Pennsylvania, Philadelphia, PA 19104; ‡Department of Psychology, Columbia University, New York, NY 10027; §Department of Ophthalmology, University of Washington, Seattle, WA 98195; and ¶Department of Ophthalmology, University of Iowa, Iowa City, IA 52242

Edited by Jeremy Nathans, Johns Hopkins University School of Medicine, Baltimore, MD, and approved March 23, 1998 (received for review February 17, 1998)

ABSTRACT **Mutations in the gene encoding rhodopsin, the visual pigment in rod photoreceptors, lead to retinal degeneration in species from *Drosophila* to man. The pathogenic sequence from rod cell-specific mutation to degeneration of rods and cones remains unclear. To understand the disease process in man, we studied heterozygotes with 18 different rhodopsin gene mutations by using noninvasive tests of rod and cone function and retinal histopathology. Two classes of disease expression were found, and there was allele-specificity. Class A mutants lead to severely abnormal rod function across the retina early in life; topography of residual cone function parallels cone cell density. Class B mutants are compatible with normal rods in adult life in some retinal regions or throughout the retina, and there is a slow stereotypical disease sequence. Disease manifests as a loss of rod photoreceptor outer segments, not singly but in microscopic patches that coalesce into larger irregular areas of degeneration. Cone outer segment function remains normal until >75% of rod outer segments are lost. The topography of cone loss coincides with that of rod loss. Most class B mutants show an inferior-nasal to superior-temporal retinal gradient of disease vulnerability associated with visual cycle abnormalities. Class A mutant alleles behave as if cytotoxic; class B mutants can be relatively innocuous and epigenetic factors may play a major role in the retinal degeneration.**

The complex pathway to blindness in human hereditary retinopathies is initiated by disease-causing mutations in genes encoding photoreceptor and retinal pigment epithelium proteins (1, 2). The first photoreceptor-specific gene found to harbor mutations was *rhodopsin* (*RHO*) (1, 3). Rhodopsin is the light-absorbing molecule that begins the signal transduction cascade in rod photoreceptors and is the best studied in the superfamily of seven transmembrane helical receptors coupled to GTP-binding proteins (4). More than 80 *RHO* mutations are now believed to cause 30% of autosomal dominant retinitis pigmentosa (RP) (3). *RHO* mutations also cause retinal degeneration in animals (5–8).

The last step to blindness in RP is programmed cell death (9–11). The intervening steps from *RHO* mutation to cell death, however, remain incompletely understood. The discovery that *RHO* mutations cause RP has prompted many laboratory investigations into disease mechanism. Subcategories of rhodopsin mutants based on biochemical properties have been defined *in vitro* (12–14), and animal models with different *RHO* mutations have been characterized (6–8). Findings from this experimental work should help to explain the visual loss in human patients and provide the basis for therapeutic intervention.

Do we know enough about the human disease resulting from *RHO* mutations to effect transfer of critical knowledge from laboratory to clinic? There have been many studies of individual genotypes but only limited attempts to synthesize data from a sizable group of patients with many different *RHO* mutations (3, 15, 16). To understand the human disease resulting from *RHO* mutations, we studied a population of patients by using noninvasive tests of rod and cone function and correlative retinal histopathology.

MATERIALS AND METHODS

Subjects. The study population consisted of 63 patients representing 18 *RHO* gene mutations. The mutations, symbols in figures (number of patients; ages at first visit) are as follows: T17M, ○ (2; 36, 68); P23H, ⊙ (13;15–73); G51A, ⊕ (4;18–63); T58R, □ (4;19–53); Q64ter, ⊡ (10;11–64); V87D, ⊞ (2; 25, 52); G89D, △ (1;16); G106R, ◬ (6;38–88); R135G, ◬ (2; 22, 47); R135L, ▽ (4;12–42); R135W, ▽ (2; 34, 46); E181K, ▽ (1; 43); D190G, ◇ (3; 33–62); T193M, ◈ (1; 49); Q312ter, ◈ (1; 64); Q344ter, ◯ (3; 24–27); V345L, ⊙ (3; 17–41); P347L, ⊕ (1; 26). Three of these patients died and retinal histopathology was performed (T17M, Q64ter, and G106R). Asymptomatic or mildly symptomatic mutation-positive patients were preferentially included; not included were patients with visual fields limited to a central island. Molecular genetic and other phenotype results from some of the patients have been reported (7, 17–25). Research procedures were in accordance with institutional guidelines and the Declaration of Helsinki.

Electroretinography (ERG). A standard ERG protocol was performed in all patients (22). Blue flashes (Wratten 47B) were used to elicit b-wave intensity series over a 3-log unit (l.u.) range up to 1.8 log scot·td·s (scotopic troland seconds). Waveforms were measured conventionally, and amplitudes were analyzed with the Naka–Rushton equation (22). High stimulus energy photoresponses were recorded in 19 patients (dark-adapted) by using one red (W26) and two blue (W47A) flashes (26). The red flash (3.6 log phot·td·s (photopic troland seconds)) was photopically matched to the higher intensity blue flash (4.6 log scot·td·s) and scotopically matched to the lower intensity blue flash (2.3 log scot·td·s). In some patients, a different stimulator was used with the same filters producing 0.2 l.u. higher energy. Acknowledging preferential effects of disease on photoreceptor type, a model of phototransduction consisting of the sum of rod and cone components (Eq. 2 in ref. 26) was used to quantify the dark-adapted waveforms. This model extends another biochemical model (27). There are two parameters each (maximum amplitude, R_{max}, and sensitivity, σ) for rod and cone components. A simplex algorithm was used to estimate the four parameters by fitting the model

The publication costs of this article were defrayed in part by page charge payment. This article must therefore be hereby marked "*advertisement*" in accordance with 18 U.S.C. §1734 solely to indicate this fact.

This paper was submitted directly (Track II) to the *Proceedings* office.
Abbreviations: *RHO*, *rhodopsin*; l.u., log unit; ROS, rod outer segment; RP, retinitis pigmentosa; ERG, electroretinography; RSL, rod sensitivity loss; CSL, cone sensitivity loss.
†To whom reprint requests should be addressed. e-mail: cideciya@mail.med.upenn.edu.

simultaneously to the three recorded responses. Components of this model have been applied previously to normal subjects (26) and patients with retinopathy (22, 25, 28).

Psychophysics. Goldmann kinetic perimetry was performed and quantified (19). Static threshold perimetry was performed in 61 patients; 71 loci (12° grid) were tested across the visual field with 500- and 650-nm stimuli (dark-adapted) and with 600-nm stimuli on a 10 cd/m^2 white background (19). Rod (at 500 nm) and cone (at 600 nm) sensitivity losses were calculated based on locus specific normal values (22). In selected patient groups, topography of sensitivity losses was summarized by mapping the frequency of occurrence of a given loss. A 3 × 3-moving average filter was applied (excluding foveal and physiological blindspot loci) before interpolating the frequency map with a cubic surface and delineating the 50th percentile contour. The process was repeated for a range of sensitivity losses and resulting contours were overlaid. Dark adaptometry after a 99% bleach (19, 20, 22) was performed in 20 patients.

Model of Rod Photoreceptor Loss in Patches. A model of the relationship between rod photoresponse and rod bipolar cell response maximum amplitudes was developed to analyze patterns of rod outer segment (ROS) loss. The model combined an ERG b-wave model (29) with morphological data on rods and rod pathway connectivity. The cell densities used were 120,000 rods/mm^2 (30), 7,000 rod bipolars/mm^2, and a rod-to-rod bipolar convergence of 60:1 (31). For simplicity, the photoreceptor and bipolar mosaics were considered to form a spatially uniform square lattice with circular receptive fields centered at each bipolar. Each rod bipolar was assumed to generate a potential that was a compressively nonlinear function of the sum of inputs from identical rods (29). When all rods within the bipolar receptive field stopped signaling, the bipolar cell ceased to contribute to the ERG b-wave. Simulations were performed on a 500 μm × 500-μm piece of "retina" divided into nonoverlapping square patches of 20, 40, 100, or 300 μm in width. To simulate an η% ROS membrane loss across the retina, all rods within a patch were made "dysfunctional" with a probability of η%. To simulate diffuse or homogeneous dysfunction, each rod cell was considered independently from its neighbors. Simulations were performed 10 times for each set of parameters, and the number of "functional" rod bipolars was plotted against "functional" rods.

Immunocytochemistry. Superior retinal regions extending from the ora serrata to the horizontal meridian were processed as flat mounts for *en face* microscopy. The retinas were from patients with T17M (68-yr-old man, FFB-316, 8.5-hr postmortem interval; ref.23), Q64ter (51-yr-old woman, FFB-424, 6.5 hr postmortem; ref. 25), and G106R (99-yr-old woman, FFB-517, 5.25 hr postmortem) *RHO* mutations and two normal adult human retinas of similar ages (54 and 76 yr) and postmortem intervals (4 and 6.5 hr). The retinas had been fixed for several days at room temperature in 4% paraformaldehyde with or without 0.5% glutaraldehyde in 0.13 M phosphate buffer, pH 7.3, and stored for up to 4 yr in 2% paraformaldehyde in the same buffer. Retinal samples were gently dissected away from the retinal pigment epithelium and processed free-floating overnight at room temperature in a mixture of primary antibodies in PBS: anti-rhodopsin (mouse mAb 1D4, 1:100; R. Molday (Univ. of British Columbia) and anti-red/green cone opsin (rabbit polyclonal antibody, 1:500; J. Saari, Univ. of Washington). The tissues were rinsed in PBS and incubated 3 hr at room temperature in a mixture of anti-mouse IgG labeled with Cy-2 (green) and anti-rabbit IgG labeled with Cy-3 (red), both from Jackson ImmunoResearch. The tissues were rinsed in PBS and mounted flat in 5% *N*-propylgallate in glycerol on microscope slides. The retinal flat mounts were examined with a Nikon microscope equipped for epifluorescence. Overlapping fields were photographed with Kodak Gold film, ASA 400, and montages were constructed from color prints. The flat mounts also were examined with a Bio-Rad MRC-600 laser-scanning confocal microscope.

RESULTS

Two Classes of Mutants. There were two patterns of rod disease expression in the patients, and there was intrafamilial consistency of pattern. Class A families (R135G, R135L, R135W, V345L, and P347L) reported onset of nightblindness in early life. Rod photoreceptor-mediated function, estimated with rod ERG b-waves and psychophysics, was severely abnormal in these patients. Class B families had one or more mutation-positive members with little or no night vision symptoms; rod b-waves were relatively preserved (33–93% of mean normal), and rod thresholds at some retinal loci were within 1.5 l.u. of normal. Some class B families, termed B1 (T17M, P23H, T58R, V87D, G106R, and D190G), had retinal regions with severe disease and other regions that were normal or far less affected. Other families, termed B2 (G51A, Q64ter, and Q344ter), showed no regional retinal predilection for disease. Patients at advanced stages of both classes were not distinguishable by retinal function testing. Classification could not be performed with certainty for four mutations in which only one family member was tested, but available data suggested that G89D and E181K probably belong to class A, and that T193M and Q312ter to class B.

Degree of Rod Disease Preceding Cone Disease: Predicting a Temporal Sequence in Class B Mutants. Rod photoresponses from a G51A patient illustrated that rod phototransduction activation could be nearly normal in some retinas that harbor a mutant allele (Fig. 1*A*). R_{max} is only slightly reduced (322 μV; normal mean ± SD = 462 ± 51 μV) with normal σ (1.51 log scot·td^{-1}·s^{-3}; normal = 1.52 ± 0.17 log scot·td^{-1}·s^{-3}). A greater loss of rod R_{max} (109 μV) is exemplified (Fig. 1*A*) by a Q64ter patient (σ = 1.17 log scot·td^{-1}·s^{-3}). Cone photoresponses in both patients were normal and nearly identical (R_{max} = 87 and 86 μV for G51A and Q64ter, respectively; normal = 77 ± 13 μV; σ = 2.2 and 2.1 log phot·td^{-1}·s^{-3}; normal = 2.6 ± 0.3 log phot·td^{-1}·s^{-3}). At disease stages when long/middle wavelength (L/M) cone photoreceptor function was normal, rod photoresponses from most patients showed reduced R_{max} with normal σ; two patients had borderline reduced σ (Fig. 1*B*). When cone

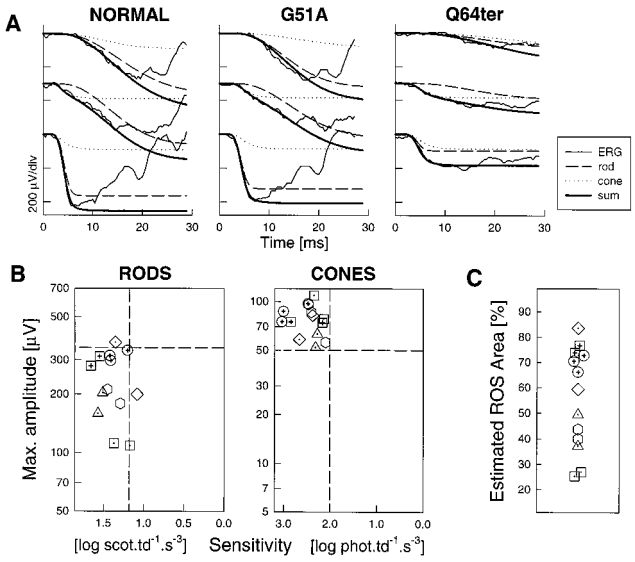

FIG. 1. Rod and cone photoreceptor physiology. (*A*) ERG photoresponses (thin lines) in a representative normal and two patients evoked by one red (middle) and two blue (top and bottom) flash stimuli. Waveforms are fitted with the phototransduction model (thick line) that is the sum of rod (dashed lines) and cone (dotted lines) components. (*B*) Summary of rod and cone photoresponse data in 13 patients; dashed lines are lower limits (mean − 2 SD) of normal. (*C*) ROS membrane area estimated (% of normal) by adjusting rod photoresponse amplitudes shown in *B* for scotomatous retinal regions by kinetic perimetry (target V-4e).

photoreceptor function was abnormal (five patients with reduced cone R_{max} and one with abnormal σ, data not shown), rod R_{max} was reduced with normal or borderline σ.

Rod R_{max} reduction can be assumed to be because of reduced ROS membrane area through loss of rod cells or decreased ROS length (32). Substantially reduced rod R_{max} in the presence of normal cone responses suggests a disease sequence: considerable rod disease occurs before the onset of secondary cone disease. An estimate from these ERG data is that L/M cones can be normal in retinas with >75% loss of ROS membrane area (Fig. 1*C*).

Topographical maps of rod sensitivity loss (RSL) and cone sensitivity loss (CSL) by psychophysics provided an opportunity to extend the electrophysiological observations on temporal sequence of rod and cone disease. Class B mutants (Fig. 2*A*) can show no RSL or CSL throughout the visual field (G51A) or in most regions outside of limited scotomatous zones (V87D). There can be relatively mild RSL across the visual field with no CSL (Q64ter). There also could be extensive scotomas (T58R) surrounded by regions with no RSL or CSL, RSL but no CSL, and varying degrees of RSL and CSL.

Locus by locus examination of these maps in patients with measurable rod function suggested a common theme, despite interindividual and intraretinal differences in severity of expression: rod disease can be considerable before cone disease is detectable. To quantify this impression, the data (18 mutations, 61 patients, 4270 loci) were divided into groups: one group for each 0.1 l.u. increment of RSL from 0 to 3.5 l.u. and a group for all RSL >3.5 l.u. The mean CSL for each of 37 groups was plotted as a function of RSL (Fig. 2*B*). Comparison of classes B1 and B2 suggested similar relationships between RSL and CSL. The degree of CSL in class A was similar to that in class B with severe rod dysfunction (Fig. 2*B*, *Inset*).

No significant change in CSL was found over the range from 0 to 1.5 l.u. of RSL (33). Specific loci that illustrate this relationship of RSL to CSL are labeled in the maps of three patients (Fig. 2*A*, arrows I and II). Starting with 1.6 l.u. of RSL, however, CSL was significantly greater when compared with groups having less RSL (locus III in T58R, Fig. 2*A*). Linear regression analysis performed in the range from 1.6 to 3.5 l.u. RSL showed a slope of 0.46 ($r^2 = 0.92$).

Topography of Rod and Cone Disease at a Macroscopic Level. Class A mutants, exemplified by V345L and R135L (Fig. 3*A*), had

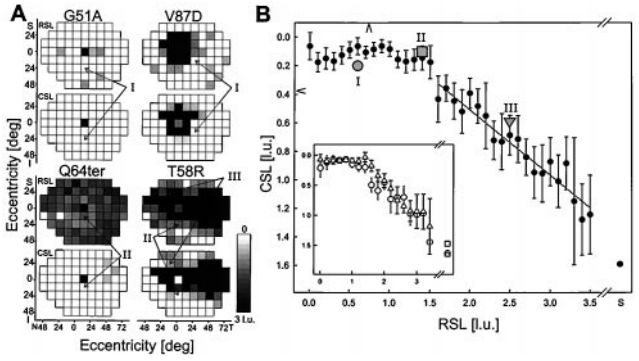

FIG. 2. Relationship between rod and cone function measured psychophysically. (*A*) Maps of RSL and CSL across the visual field of four patients displayed on a gray scale. All maps are displayed as right eyes: superior (S), inferior (I), nasal (N), and temporal (T) fields. White is normal; black is >3 l.u. of sensitivity loss for rods, unmeasurable for cones; physiological blindspot is shown as black at 12°T. Representative loci are marked with no RSL or CSL (I); RSL but no CSL (II); and combined RSL and CSL (III). (*B*) Mean CSL as a function of RSL (●); error bars are ± 1 SEM. The loci marked in *A* are shown with gray symbols. Arrowheads against axes denote lower limits of normal (mean − 2 SD) averaged across the visual field. Gray line is the linear regression applied to the data in the range from 1.6 through 3.5 l.u. of RSL. (*Inset*) Three subsets of the patient population: Class A ($n = 12$, □); Class B1 ($n = 29$, ○) and B2 ($n = 16$, △).

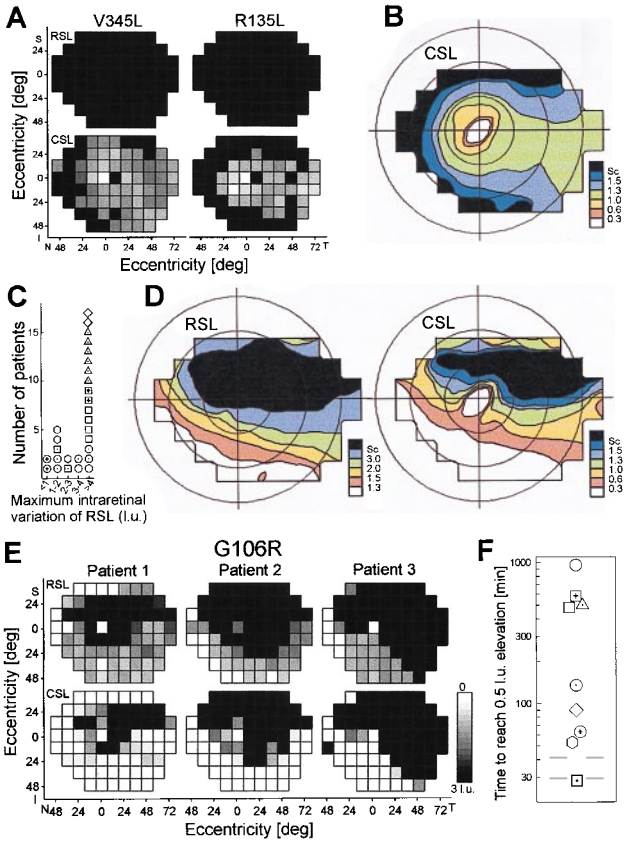

FIG. 3. Topographical variation of rod and cone dysfunction. (*A*) Maps of RSL and CSL in two class A patients, V345L and R135L, displayed in Fig. 2*A*. (*B*) Summary contour map of CSL in eight class A patients displaying 50th percentile contours of selected sensitivity losses; the loss in l.u. for each contour shown on the color scale (Sc, scotoma); isoeccentricity lines are 20, 40, and 60°. Maps are shown as a visual field of the right eye. (*C*) Histogram of the maximum intraretinal variation of RSL in 28 class B patients with relatively mild dysfunction (<1.5 l.u. of RSL in some retinal regions). (*D*) Summary contour maps of RSL and CSL for 16 class B patients showing >3 l.u. of intraretinal RSL variation. (*E*) Maps of RSL and CSL in three family members with the G106R mutation having increasing (left to right) degrees of disease severity (displayed as in Fig. 2*A*). (*F*) Dark adaptation kinetics of class B disease, representing nine mutations. Each symbol is the time to recover to within 0.5 l.u. of prebleach sensitivity after a 99% bleach; results of two to three least affected patients of each mutation are averaged. Gray lines show the normal limits.

severe rod dysfunction across the retina but measurable cone function. What is the cone function topography in these retinas with early loss of most or all rod function? A contour map of CSL (Fig. 3*B*) in eight patients (1–3 least affected for R135G, R135L, R135W, V345L, and P347L) indicates greatest cone function centrally with an elongate band of function extending into the temporal peripheral field.

Class B1 mutants, formally defined as having >3 l.u. of intraretinal variation of RSL (Fig. 3*C*), have measurable rod as well as cone topography. Contour maps summarizing rod and cone function in 16 class B1 patients (2–3 least affected for T17M, P23H, T58R, V87D, G106R, and D190G) demonstrate a superior-temporal to inferior-nasal field gradient of vulnerability (Fig. 3*D*). The most vulnerable region for rods extends from central to superior peri-central field and the least vulnerable is the inferonasal peripheral field. Cone results tend to follow those of the rods except at the fovea. In class B2 patients (showing <3 l.u. intraretinal RSL variation, Fig. 3*C*), there were no evident topographical features for RSL or CSL (data not shown). Of interest, P23H showed both class B1 and B2 behavior.

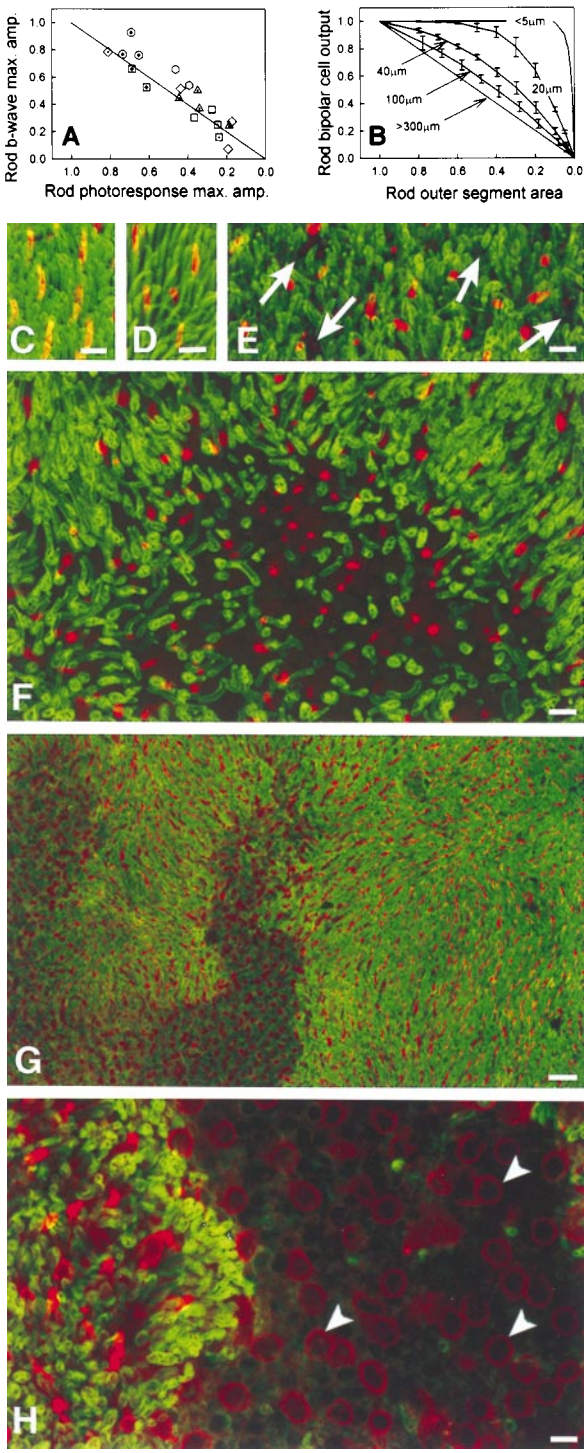

FIG. 4. Evidence for microscopic patches of photoreceptor disease. (*A*) Rod ERG b-wave maximum amplitude plotted against rod photoresponse maximum amplitude; both measures are shown as fraction of mean normal. Line represents equal reduction of the two variables. (*B*) Computational model of rod bipolar output as a function of ROS area shown as fractions of normal; curves are labeled by the size of the dysfunctional patches used in the simulations, error bars are ± 2 SD (*C-H*) Flat mount preparations of the superior regions of human retinas. ROS have been immunolabeled with anti-rhodopsin (green), and COS have been labeled with anti-red/green cone opsin (red). Calibration bars indicate 10 μm in *C-F* and *H* and 20 μm in *G*. (*C*) Periphery of normal human retina. (*D*) Far periphery (3 mm from ora serrata) of G106R retina showing near normal ROS and COS. (*E*) Periphery (5 mm from ora serrata) of T17M retina showing shortening of ROS and COS and presence of small gaps (arrows) in the layer of ROS. (*F*) Periphery (10 mm from ora serrata) of T17M retina showing a larger patch of ROS loss; retained COS are short. (*G*) Low magnification of G106R mid-periphery with larger patches that contain no ROS. (*H*) High magnification of a region in G. Within a rod-free patch, only cone somata (arrowheads) are retained. Their surface membrane are cone opsin positive. Short ROS and COS are present near the edge of the rod-free patch.

The gradient of increasing disease across the visual field in class B1 mutants is evident in individual maps of affected family members, exemplified in the G106R mutation (Fig. 3*E*). Patient 1 has various degrees of RSL across the field and scotomas in pericentral and supero-temporal regions; patients 2 and 3 had more extensive rod scotomas occupying the superior and temporal fields with preservation of rod function infero-nasally. CSL was less extensive than RSL but in the same spatial distribution in all three patients.

Are rods entirely normal in the least vulnerable retinal regions of class B1 mutants or throughout the retina of some class B2 mutants? In 20 patients representing nine mutations, the kinetics of dark adaptation were measured at loci with normal sensitivity or <1 l.u. RSL. All class B mutants except Q64ter had abnormal dark adaptation. Class B1 have much longer delays in recovery compared with class B2 (Fig. 3*F*).

Topography of Rod and Cone Disease at a Microscopic Level in Class B Mutants. In class B, the relationship between rod photoresponse and b-wave maximum amplitudes concentrates along the line predicting equal fractional loss of both measures (Fig. 4*A*). Loss of photoreceptor function in large retinal regions, as in some class B1 patients, can lead to concomitant loss of both amplitudes, assuming a direct relationship between rod photoresponses and the circulating current of rod cells (32) as well as between rod ERG b-waves and rod bipolar responses (34). The equal losses of amplitude in class B2 patients, however, are not as easily explained; their psychophysical data do not show macroscopic patches of receptor-mediated loss. A truly homogeneous loss of ROS membrane would be expected to reduce photoresponse amplitudes more than b-wave amplitudes (35). Further, adjustment of R_{max} by the relative extent of scotomatous areas in class B1 patients (Fig. 1*C*) showed that the large scotomas were not the sole cause of R_{max} reduction.

What is the microscopic topography of rod dysfunction in retinal regions that macroscopically have homogeneous dysfunction? A model of an idealized retina that takes into account the convergence of signals from rods to rod bipolars was used to estimate the maximum output of rod bipolars as a function of ROS membrane area loss in microscopic patches of different size (Fig. 4*B*). When the patch size is smaller than the receptive field of rod bipolars, large reductions in ROS area cause negligible reductions in rod bipolar output. However, as the patch extent increases, the relationship between ROS area and rod bipolar output moves toward being linear. Comparison of Fig. 4 *A* and *B* rules out homogeneous loss of ROS in class B patients; the ERG data are consistent with patchy loss of ROS with patch sizes exceeding 40 μm × 40 μm. To test this hypothesis, we examined donor retinas from patients with *RHO* mutations.

In the G106R retina, the superior far periphery contained rods and cones with OS of near normal length (ROS: ≈20 μm; COS: ≈13 μm) (Fig. 4*D*). The OS shortened over a gradient, and in the mid-periphery, the ROS were ≈5 μm or less and the COS were ≈10 μm or less. Small gaps were present in the ROS mosaic reflecting loss of individual or small groups of rods. In addition, larger patches contained no rods and only cone somata with short to absent COS (Fig. 4 *G* and *H*). These patches were very irregular in shape (Fig. 4*G*), perhaps formed by coalescence of smaller patches over time.

The T17M retina had similar findings. The superior far periphery contained near normal numbers of rods and cones with approximately normal OS length (ROS: ≈20 μm; COS: ≈13 μm). OS lengths gradually shortened in a gradient from far

toward mid-periphery, whereas ROS lengths were ≈10 μm or less and COS were 6.5 μm or less. Small gaps were apparent in the layer of ROS, reflecting loss of rods (Fig. 4*E*). Larger gaps also were present in the photoreceptor mosaic (Fig. 4*F*), reflecting death of nearly all rods within a patch. These patches were variable in shape and size, measuring ≈160 μm or more in diameter. Cone cells were retained within these larger patches, but their OS were very short (Fig. 4*F*).

In the Q64ter retina (not shown), the superior far periphery contained greatly reduced numbers of rods and cones with very short or absent OS. Essentially, no rods or cones were present in the mid periphery. The few remaining rod somata in the far periphery were grouped in clusters, whereas the cone somata were scattered singly.

DISCUSSION

Classes of Disease Phenotype and *in Vitro* Biochemistry. Two classes of rod disease behavior in autosomal-dominant RP caused by *RHO* mutations were found in this study, corroborating many similar observations (3). Class A shows severe retina-wide loss of rod function from relatively early in life. This class of mutants leads to a disease phenotype that could be expected from cytotoxic heterozygous alleles or homozygous loss-of-function mutations (4, 36, 37). Autosomal recessive RP caused by mutations in another rod-specific gene encoding a phototransduction protein—β subunit of phosphodiesterase—also shows this phenotype (38). Class B, in contrast, can show normal ROS length, rod activation kinetics, and sensitivity throughout the retina or in some regions; most patients have allele-specific abnormalities in the rod visual cycle measured by dark adaptation kinetics. The milder phenotype in class B is more in keeping with a loss-of-function mutation inherited in single dose (37).

The relationship between *in vitro* biochemical classes of rhodopsin mutants and the human disease classes is undoubtedly complex. It is of interest that the three different substitutions at codon 135 associated with class A involve the highly conserved structure at the interface between transmembrane segment III and cytoplasm in G protein-coupled receptors (39, 40). *In vitro* studies show defective folding or stability (12, 13) as well as loss of G protein activation (39). How a single copy of a mutant leads to a relatively rapid loss of all rod vision and degeneration is not known. Most class B disease mutants show folding and/or stability abnormalities *in vitro* (12–14). These single copy defects, although compatible with normal ROS length, sensitivity, and activation kinetics, may manifest defective rhodopsin biochemistry at a phenotypic level by abnormal rod dark adaptation kinetics (20).

A Disease Sequence For Rod Photoreceptors. Normal rods in some retinal regions or throughout the retina in class B mutants indicate that ROS can develop normally and maintain OS length (sometimes well into adult life) in the presence of the mutant allele and the attendant biochemical defects. There are two sequential and shared pathological consequences associated with a mutant allele in a rod cell: ROS shortening and subsequent cell death by apoptosis (41). Results in this study indicate that there are definable steps in the disease sequence after ROS reduction becomes detectable and before all rod and cone function is lost. We found that when ROS membrane loss occurs, it is not by uniform shortening of OS length but in patches. The disease progresses by further ROS loss and coalescence of patches, leading eventually to rod scotomas.

This rod disease sequence is not unique to *RHO* mutations. Shortening of ROS is common to many hereditary retinal degenerations (41, 42) and suggested to result from abnormal disk membrane morphogenesis (43). A patchy pathological process at a microscopic level has been reported, albeit rarely. Clusters of surviving receptors have been noted in some murine retinal degenerations not caused by *RHO* mutations (44, 45). Previous ERG studies in RP patients of various genetic types also suggest micropatches of photoreceptor disease (35). The basis for small dysfunctional patches among normally functioning rods is unclear, but it could be caused by local interdependence of rods on other rods or neighboring cells (46, 47). Such cellular interactions could be trophic or toxic (48), with either effect leading to geographic patterns of disease from diffusion of factors.

Inferior–Superior Retinal Disease Gradient. Class B1 disease tends to be inhomogeneous not only at a microscopic level but also at a macroscopic level. Many patients show an inferior–superior retinal gradient of disease expression (3). The gradient we found tends to be diagonal across the retina, most severe in the pericentral and infero-nasal retina, and least severe in supero-temporal retina. There was allele specificity for the gradient; the topography of increasing disease expression within a family resembled the summary data from many mutations. Class B2 patients did not show major intraretinal variation in rod sensitivity, and there was no obvious gradient. Patients with the P23H mutation are of interest because some showed variation whereas others did not. The latter had mild rod dysfunction when evaluated and may represent a stage of disease before a detectable macroscopic disease focus.

We propose that the gradient results from intraretinal variation in rate of the stereotypical rod disease sequence outlined above: the relationship between RSL and CSL at retinal loci in areas of high and low vulnerability are the same and best demonstrated in mildly affected patients in families with the gradient. What could accelerate rod disease unevenly across a retina composed of rods all with the same mutant allele? One hypothesis, bolstered by experimental evidence in a murine model with a *RHO* mutation, is that light exposure accelerates rod disease rate unevenly across the retina (23, 49, 50). It is noteworthy that class B patients with the gradient have greater prolongation of dark adaptation kinetics than those without a gradient. Allele specificity of the gradient within class B disease may be related to this difference in rod recovery rate after light exposure. Rods with certain mutant alleles, when exposed to environmental light, may behave as if chronically activated and thereby experience a form of light damage; retinal regions with potentially greater light exposure, like the inferior retina, could be damaged more rapidly (23). Experimental light damage can be mediated through rhodopsin and cause retinal degeneration with regional retinal differences in severity (51).

Inferior–superior retinal gradients of vulnerability, like the microscopic patches of rod disease, are not specific to *RHO* mutations or retinopathies with prolonged dark adaptation. Similar patterns have been found in other forms of retinal degeneration in humans and animals (3, 42, 52–55), including heterozygotes of X-linked RP (56). The latter may be another example of microscopic patchiness of retinal degeneration (caused by X inactivation) leading to a similar topographic pattern of disease. Interestingly, there are orderly dorso-ventral molecular gradients during normal retinal development and postnatally (57–60). Any of a number of retina-wide gradients, as part of the genetic background of some individuals, could act to modify the effects of a disease gene. The gradient in *RHO* mutations is likely to result from an interplay between mutant allele, other genetic and epigenetic factors, one of which may be environmental light.

Secondary Cone Disease Depends on the Spatial and Temporal Sequence of Rod Disease. In class B mutants, cone dysfunction was detectable only in retinas (by ERG) or at individual retinal loci (by psychophysics) that had a loss of at least 75% of ROS. Once cone function was detectable, it declined 3.5 times slower than rods. Extrapolation from these cross-sectional data suggests a temporal dependence of cone disease on the extent of rod pathology (61). Cone cells can retain normal function until a certain percentage of rods are sufficiently affected by disease. The decrease in cone function, once initiated, occurs at a slower rate than that of rods.

A spatial dependence of cone on rod disease is evident in the topographical maps of class B1 mutants. Summary contour maps

of RSL and CSL are comparable in all regions except the central retina, where the high density of foveal cones modifies the contours.

Temporal and spatial dependence of cone survival on rods lends support to hypotheses of trophic interactions between photoreceptors. Cone survival also may be jeopardized by progressive abnormalities in surrounding cells and the extracellular environment as a consequence of increasing rod disease (11, 46–48, 62).

Class A mutants with unmeasurable rod function had a cone contour map resembling cone cell density maps in humans (30), suggesting a constant rate of cone disease progression across the retina. Although mean cone dysfunction at loci with unmeasurable rod function was similar in classes A and B, there was a notable difference on inspection of individual maps. In class B1, cone function was not detectable within inferior retinal rod scotomas. In contrast, class A had measurable cone function across large regions of retina devoid of rod function. It is possible that the mechanism of secondary cone degeneration may differ in class A and B retinas.

Future Studies and Therapeutic Implications. The present results in man raise a number of questions best answered by experimental studies. The basis of the two classes of mutants, the microscopic inhomogeneities and retina-wide gradients of rod disease, and the dependence of cone survival on degree and location of rod disease seem potentially explorable *in vitro* (12–14) and *in vivo* (5–8). Our extrapolated cross-sectional results suggesting longitudinal trends require confirmation by natural history studies.

Therapeutic needs may be quite different for the two classes of disease. In class A, the early catastrophic loss of rod function may not be correctable and efforts may be better focused on promoting cone cell survival. In class B, rod loss may be responsive to control of environmental risk factors and maintenance of rod function may ultimately be the best strategy to prevent cone loss.

We are grateful to Dr. J. Nathans for mutation analyses; Dr. M. Maguire for statistical consultation; A. and M. Roman for allowing inclusion of their patients in the data analyses; K. Zhao for computer programming; and Dr. C. Kemp, Dr. J. Huang, I. Klock, D. Possin, M. Benegas, D. Hanna, H. Heo, D. Slaughter, K. Stewart, and B. Koernig for help with the study. This work was supported in part by Public Health Service research grants (EY-05627, 01311, 01730, 08426, and 09076), the Foundation Fighting Blindness (Hunt Valley, MD), the Whitaker Foundation (Rosslyn, VA), the Chatlos Foundation, Inc. (Longwood, FL), F. M. Kirby Foundation, and the Mackall Trust.

1. Dryja, T. P. & Li, T. (1995) *Hum. Mol. Genet.* **4,** 1739–1743.
2. Farber, D. B. & Danciger, M. (1997) *Curr. Opin. Neurobiol.* **7,** 666–673.
3. Gal, A., Apfelstedt-Sylla, E., Janecke, A. R. & Zrenner, E. (1997) *Prog. Retinal Eye Res.* **16,** 51–79.
4. Spiegel, A. M. (1997) *J. Inherit. Metab. Dis.* **20,** 113–121.
5. Pak, W. L. (1995) *Invest. Ophthalmol. Visual Sci.* **36,** 2340–2357.
6. Colley, N. J., Cassil, J. A., Baker, E. K. & Zuker, C. S. (1995) *Proc. Natl. Acad. Sci. USA* **92,** 3070–3074.
7. Petters, R. M., *et al.* (1997) *Nat. Biotechnol.* **15,** 965–970.
8. Travis, G. H. (1997) *Nat. Genet.* **15,** 115–117.
9. Li, Z.-Y. & Milam, A. H. (1995) in *Retinal Degeneration II*, eds. Anderson, R. E., Hollyfield, J. G. & LaVail, M. M. (Plenum, New York), pp. 1–12.
10. Adler, R. (1996) *Arch. Ophthalmol.* **114,** 79–83.
11. Wong, F. (1997) *Prog. Retinal Eye Res.* **16,** 353–373.
12. Sung, C.-H., Schneider, B. G., Agarwal, N. & Papermaster, D. S., Nathans, J. (1991) *Proc. Natl. Acad. Sci. USA* **88,** 8840–8844.
13. Sung, C.-H., Davenport, C. M. & Nathans, J. (1993) *J. Biol. Chem.* **268,** 26645–26649.
14. Kaushal, S. & Khorana, H. G. (1994) *Biochemistry* **33,** 6121–6128.
15. Daiger, S. P., Sullivan L. S. & Rodriguez J. A. (1995) *Behav. Brain Sci.* **18,** 452–467.
16. Sandberg, M. A., Weigel-DiFranco C., Dryja, T. P. & Berson E. L. (1995) *Invest. Ophthalmol. Visual Sci.* **36,** 1934–1942.
17. Tucker, G. S. & Jacobson, S. G. (1988) *Retina* **8,** 30–41.
18. Sung, C.-H., Davenport, C. M., Hennessey, J. C., Maumenee, I. H., Jacobson, S. G., Heckenlively, J. R., Nowakowski, R., Fishman, G., Gouras, P. & Nathans, J. (1991) *Proc. Natl. Acad. Sci. USA* **88,** 6481–6488.
19. Jacobson, S. G., Kemp, C. M., Sung, C.-H. & Nathans, J. (1991) *Am. J. Ophthalmol.* **112,** 256–271.
20. Kemp, C. M., Jacobson, S. G., Roman, A. J., Sung, C.-H. & Nathans, J. (1992) *Am. J. Ophthalmol.* **113,** 165–174.
21. Macke, J. P., Davenport, C. M., Jacobson, S. G., Hennessey, J. C., Gonzalez-Fernandez, F., Conway, B. P., Heckenlively, J., Palmer, R., Maumenee, I. H., Sieving, P., *et al.* (1993) *Am. J. Hum. Genet.* **53,** 80–89.
22. Jacobson, S. G., Kemp, C. M., Cideciyan, A. V., Macke, J. P., Sung, C.-H. & Nathans, J. (1994) *Invest. Ophthalmol. Visual Sci.* **35,** 2521–2534.
23. Li, Z.-Y., Jacobson S. G. & Milam A. H. (1994) *Exp. Eye Res.* **58,** 397–408.
24. Rosas, D. J., Roman, A. J., Weissbrod, R., Macke, J. P. & Nathans, J. (1994) *Invest. Ophthalmol. Visual Sci.* **35,** 3134–3144.
25. Milam, A. H., Li, Z.-Y., Cideciyan, A. V. & Jacobson, S. G. (1996) *Invest. Ophthalmol. Visual Sci.* **37,** 753–765.
26. Cideciyan, A. V. & Jacobson, S. G. (1996) *Vision Res.* **36,** 2609–2621.
27. Lamb, T. D. & Pugh, E. N., Jr. (1992) *J. Physiol.* **449,** 719–758.
28. Cideciyan, A. V., Zhao, X., Nielsen, L., Khani, S. C., Jacobson, S. G. & Palczewski, K. (1998) *Proc. Natl. Acad. Sci. USA* **95,** 328–333.
29. Hood, D. C., Shady, S. & Birch, D. G. (1994) *Invest. Ophthalmol. Visual Sci.* **35,** 2477–2488.
30. Curcio, C. A., Sloan, K. R., Kalina, R. E. & Hendrickson, A. E. (1990) *J. Comp. Neurol.* **292,** 497–523.
31. Grunert, U. & Martin, P. R. (1991) *J. Neurosci.* **11,** 2742–2758.
32. Hood, D. C. & Birch, D. G. (1994) *Invest. Ophthalmol. Visual Sci.* **35,** 2948–2961.
33. Mansfield, J. S., Legge, G. E. & Bane, M. C. (1996) *Invest. Ophthalmol. Visual Sci.* **37,** 1492–1501.
34. Hood, D. C. & Birch, D. G. (1996) *J. Opt. Soc. Am. A* **13,** 623–633.
35. Shady, S., Hood, D. C. & Birch, D. G. (1995) *Invest. Ophthalmol. Visual Sci.* **36,** 1027–1037.
36. McInnes, R. R. & Bascom, R. A. (1992) *Nat. Genet.* **1,** 1–3.
37. Coughlin, S. R. (1994) *Curr. Opin. Cell Biol.* **6,** 191–197.
38. Danciger M., Heilbron, V., Gao, Y.-Q., Zhao, D.,-Y., Jacobson, S. G. & Farber, D. B. (1996) *Mol. Vision* **2,** 10.
39. Min, K. C., Zvyaga, T. A., Cypess, A. M. & Sakmar, T. P. (1993) *J. Biol. Chem.* **268,** 9400–9404.
40. Birnbaumer, M. (1995) *J. Recept. Signal Transduct. Res.* **15,** 131–160.
41. Milam, A. H., Li, Z.-Y. & Fariss, R. N. (1998) *Prog. Retinal Eye Res.*, in press.
42. Aguirre, G. (1996) in *Great Basin Visual Science Symposium* (University of Utah, Salt Lake City), pp. 6–21.
43. Liu, X., Wu, T. H., Stowe, S., Matsushita, A., Arikawa, K., Naash, M. I. & Williams, D. S. (1997) *J. Cell Sci.* **110,** 2589–2597.
44. Campochiaro, P. A., Chang, M., Ohsato, M., Vinores, S. A., Nie, Z., Hjelmeland, L., Mansukhani, A., Basilico, C. & Zack, D. J. (1996) *J. Neurosci.* **16,** 1679–1688.
45. Blanks, J. C., Spee, C., Barron, E., Rich, K. A. & Schmidt, S. (1997) *Curr. Eye Res.* **16,** 733–737.
46. Milam, A. H. (1993) *Curr. Opin. Neurobiol.* **3,** 797–804.
47. Steinberg, R. (1994) *Curr. Opin. Neurobiol.* **4,** 515–524.
48. Huang, P. C., Gaitan, A. E., Hao, Y., Petters, R. M. & Wong, F. (1993) *Proc. Natl. Acad. Sci. USA* **90,** 8484–8488.
49. Heckenlively, J. R., Rodriguez, J. A. & Daiger, S. P. (1991) *Arch. Ophthalmol.* **109,** 84–91.
50. Naash, M. L., Peachey, N. S., Li, Z.-Y., Gryczan, C. C., Goto, Y., Blanks, J., Milam, A. H. & Ripps, H. (1996) *Invest. Ophthalmol. Visual Sci.* **37,** 775–782.
51. Organisciak, D. T. & Winkler, B. S. (1994) *Prog. Retinal Eye Res.* **13,** 1–29.
52. LaVail, M. M. & Battelle, B.-A. (1975) *Exp. Eye Res.* **21,** 167–192.
53. Massof, R. W. & Finkelstein, D. (1981) *Doc. Ophthalmol.* **51,** 289–346.
54. Fishman, G. A., Alexander, K. R. & Anderson, R. J. (1985) *Arch. Ophthalmol.* **103,** 366–374.
55. LaVail, M. M., Matthes, M. T., Yasumura, D. & Steinberg, R. H. (1997) *Exp. Eye Res.* **65,** 45–50.
56. Fishman, G. A., Weinberg, A. B. & McMahon, T. (1986) *Arch. Ophthalmol.* **104,** 1329–1335.
57. Barnstable, C. J. (1987) *Mol. Neurobiol.* **1,** 9–46.
58. Zack, D. J., Bennett, J., Wang, Y., Davenport, C., Klaunberg, B., Gearhart, J. & Nathans, J. (1991) *Neuron* **6,** 187–199.
59. Lem, J., Applebury, M. L., Falk, J. D., Flannery, J. G. & Simon, M. I. (1991) *Neuron* **6,** 201–210.
60. Drager, U. C. & McCaffery, P. (1997) *Prog. Retinal Eye Res.* **16,** 323–351.
61. Nusinowitz, S. & Birch, D. G. (1997) in *Basic and Clinical Applications of Vision Science*, ed. Lakshminarayanan, V. (Kluwer, Dordrecht), pp. 237–240.
62. Li, Z.-Y., Chang J. H. & Milam A. H. (1997) *Visual Neurosci.* **14,** 671–679.